Translational Oncology
www.transonc.com

Volume 12 Number 8 August 2019 pp. 1056–1071 1056

Characterization of Novel Murine and Human PDAC Cell Models: Identifying the Role of Intestine Specific Homeobox Gene *ISX* in Hypoxia and Disease Progression[1]

Arsheed A. Ganaie[*,2], Aijaz Parray[*,†,2], Tabish Hussain[*,‡], Ashraf Shabaneh[§], Anmbreen Jamroze[¶], Marina G. Ferrari[*], Lei Wang[#], D. Joshua Liao[#], Shahriar Koochekpour[**], Sanjeev Nanda[††], Jinhua Wang[§], Yibin Deng[#], Sergio A Gradilone[‡‡], Edward H. Hinchcliffe[§§], Badrinath R. Konety[*] and Mohammad Saleem[*]

[*]Department of Urology, Masonic Cancer Center, University of Minnesota, Minneapolis, MN; [†]Translational Research Institute, Academic Health Systems Hamad Medical Corporation, Doha, Qatar; [‡]MD Anderson Cancer Center, Science Park, Smithville, TX; [§]Institute for Health Informatics, Masonic Cancer Center, University of Minnesota, Minneapolis, MN; [¶]Hormel Institute, University of Minnesota, Austin, MN; [#]Department of Cancer Genetics, Hormel Institute, University of Minnesota, Austin, MN; [**]Department of Urology, University of Florida, Jacksonville, Florida; [††]Department of General Internal Medicine, Mayo Clinic, Rochester, MN; [‡‡]Cancer Cell Biology and Translational Research Section, Hormel Institute, University of Minnesota, Austin, MN; [§§]Cellular Dynamics Section, The Hormel Institute, University of Minnesota

Abstract

Therapy failure and metastasis-associated mortality are stumbling blocks in the management of PDAC in patients. Failure of therapy is associated to intense hypoxic conditions of tumors. To develop effective therapies, a complete understanding of hypoxia-associated changes in genetic landscape of tumors during disease progression is needed. Because artificially immortalized cell lines do not rightly represent the disease progression, studying genetics of tumors in spontaneous models is warranted. In the current study, we generated a spectrum of spontaneous human (UM-PDC1; UM-PDC2) and murine (HI-PanL, HI-PancI, HI-PanM) models representing localized, invasive, and metastatic PDAC from a patient and transgenic mice (*K-ras*^{G12D}/*Pdx*^{cre}/*Ink4a/p16*$^{-/}$). These spontaneous models grow vigorously under hypoxia and exhibit activated K-ras signaling, progressive loss of PTEN, and tumorigenicity *in vivo.* Whereas UM-PDC1 form localized tumors, the UM-PDC2 metastasize to lungs in mice. In an order of progression, these models exhibit genomic instability marked by gross chromosomal rearrangements, centrosome-number variations, Aurora-kinase/H2AX colocalization, loss of primary cilia, and α-tubulin acetylation. The RNA sequencing of hypoxic models followed by qRT-PCR validation and gene-set enrichment identified Intestine-Specific Homeobox factor (*ISX*)–driven molecular pathway as an indicator PDAC aggressivness. TCGA-PAAD clinical data analysis showed high *ISX* expression correlation to poor survival of PDAC patients, particularly women. The functional studies showed *ISX* as a regulator of i) invasiveness and migratory potential and ii) *VEGF*, *MMP2*, and NFκB activation in PDAC cells. We suggest that ISX is a potential druggable target and newly developed spontaneous cell models are valuable tools for studying mechanism and testing therapies for PDAC.

Translational Oncology (2019) 12, 1056–1071

Address all correspondence to: Mohammad Saleem, PhD, Associate Professor, Department of Urology, Masonic Cancer Center, University of Minnesota, 2231, 6th St. SE, Minneapolis, MN. E-mail: msbhat@umn.edu

[1] Conflict of Interest Statement: no conflict.

[2] Authors contributed equally.

Received 26 April 2019; Revised 3 May 2019; Accepted 3 May 2019

1936-5233/19
https://doi.org/10.1016/j.tranon.2019.05.002

Introduction

Majority of the pancreatic cancer (PDAC) cases are diagnosed as metastatic disease, whereas only 10%-15% of the cases are recommended for surgery, the only standard care available to such patients [1]. PDAC patients exhibit poor prognosis with a median survival time of <6 months, and approximately 85% therapy-receiving patients develop drug resistance and recurrent disease [2,3]. The failure of conventional therapies can be attributed to an incomplete understanding of the complex pathophysiology of disease and absence of reliable diagnostic/or prognostic markers [4,5]. It is believed that for the early detection and effective treatment, a complete understanding of molecular basis of PDAC progression is required. To study the molecular mechanism underlying PDAC, cell line models exhibiting either wild-type K-ras (BxPC3, Hs766T) or mutant K-ras (PanC1, AsPC1, MIA PaCa-2, Capan-1, Capan-2, HPAC, HPAF-II, SU-86.86) expression have been used by investigators [6]. These cell models display disparate genotypes and phenotypes [6]. In addition, majority of the mentioned models are artificially immortalized, represent one unique stage of disease, and are of multipatient origin. These limitations preclude the use of immortalized models for studying disease progression. There is a need to develop spontaneous models (without artificial immortalization) which belong to same genetic background, show phenotype changes over a period of time, and mimic disease progression. In this study, we established spontaneous i) human models representing localized and metastatic PDAC and ii) *K-ras*^{G12D}/*p16*$^{-/-}$ background spontaneous murine models progression model (representing localized, primary invasive, and metastatic stage, respectively). We studied the gross changes in the i) genomic stability and ii) genetic landscape in pancreatic neoplastic cells when the disease progresses from localized to metastatic form.

The dysregulation in the activities of various of transcriptional factors during the progression of PDAC in humans is a common event [7]. However, the critical transcriptional factors which are required for acquiring of metastasis phenotype or driving of metastasis of pancreatic carcinoma cells are poorly understood. The Homeo domain containing transcription factors family plays significant role in the differentiation and morphogenesis during early embryonic development, and dysegulation of homeobox gene expression (resulting in hyper cell proliferation) has been reported in several human cancers [8]. Based on the RNA sequencing of pancreatic cell models, we identified Intestine Specific Homeobox gene (ISX) transcriptional factor critical for progression of PDAC from localized to metastasis. We investigated the critical role played by ISX in acquiring the metastatic phenotype by PDAC cells. Using PDAC patient specimens, human/murine models, bioinformatics, and publically vailable Cancer Genome data, we establish the relevance of *ISX*-driven molecular signature as a novel disease staging marker and a potential therapeutic target for treating metastatic PDAC.

Material and Methods

Antibodies and Plasmids

Pancreatic marker antibody set (anti–α-amylase, anti-PDX1, and anti-PLA2GB), anti-ERK, anti-p38, anti-AKT, anti–phospho-AKT, anti-NFκB, anti–phospho-NFκB-p65, anti–E-Cadherin, anti–Cytokeratin-8, anti-vimentin, anti-PCNA, anti-PTEN, and anti–β-actin antibodies were procured from Cell Signaling technology (Danvers, MA). Anti-VEGF antibody was purchased from Santa Cruz laboratories (Dallas, TX). Anti–K-ras-GTP and anti–K-ras antibodies were purchased from NewEast Biosciences Labs (King of Prussia, PA). Anti-ISX antibody was purchased from Novus biologicals (Littleton, CO). Anti–acetylated-α-tubulin antibody was purchased from Sigma (St. Louis, MO). Reporter plasmids *pGL3-VEGF* and *pGL3-MMP2* were obtained from a plasmid repository (Addgene, Cambridge, MA).

Cell Culture

ASPC1 cells were purchased from ATCC and cultured in RMP1 medium. HI-PanL, HI-PancI, HI-PancM, and UM-PDC cell models were generated and characterized by us. The cell models were characterized for chromosome number (karyotyping) at Roswell Park Cancer Institute (Buffalo, NY) and Cytogenomics Core Laboratory of Masonic Cancer Center, University of Minnesota. Human UM-PDC1 and UM-PDC2 cell lines developed in our laboratory are maintained in DMEM culture medium. All cell lines were authenticated for human and mouse STR Profiling at Genetica Cell Line Testing, (Burlington, NC).

Human Patient Tumor

The pancreatic tumors of PDAC patient (nonidentifiable) who underwent the surgery at the Vanderbilt University (Nashville, TN) was procured through National Cancer Institute–supported Cooperative Human Tissue Network.

Transgenic Mouse Breeder Colonies

The breeder pairs of genetically engineered mouse models belonging to genotype *LSL-K-ras*^{G12D} *(LSL-K-ras*^{tm3Tyj}/Nci), *PDX1*^{cre}, and *Ink4a/Arf null* (*Cdkn2a*^{tm1Rdp}/) mice were procured from NCI/NIH mouse repository (Fredrick, Baltimore). The breeding and genotyping were performed as per vendors' instructions. The information about the primer combinations used for genotyping by using PCR method is provided in the Supplementary Figure 1*A*.

Generation of Transgenic K-ras^{G12D} *Pdx*^{Cre} *p16*$^{-/-}$ *Mice*

For the targeted expression of oncogenic *K-ras* in pancreas, *K-ras*^{G12D} *Pdx*^{Cre} transgenic mouse models as described by Bardeesy et al. ' and Hingorani et al. [9,10] were used. Briefly, a mouse model expressing a Cre-activated *K-ras*^{G12D} allele inserted into the endogenous *K-ras* locus, and these mice were crossed with mice expressing Cre recombinase in pancreatic tissue by virtue of a *PDX-1* promoter-driven transgene. The subsequent recombination resulted in interbreeding *K-ras*^{G12D} mice with animals that express Cre recombinase from the pancreatic-specific promoters *PDX-1*. The loss of functional G1 cyclin-dependent kinase inhibitor Ink4a/*p16* is the universal event of PDAC; however, constitutive deletion of only Ink4a/*p16* is not sufficient to develop advanced stages of PDAC. Therefore, with cross-breeding between *K-ras*^{G12D} *Pdx*^{Cre} and *p16*$^{-/-}$ mice was performed to generate transgenic *K-ras*^{G12D}*Pdx*^{Cre}/*p16*$^{-/-}$genotype mice which exhibit an earlier appearance of PanIN lesions followed by rapid progression into highly invasive and metastatic PDAC. All transgenic mice were tested for parent *K-ras* mutation and *p16*$^{-/-}$ deletion (Supplementary Figure 1, *B-C*).

Generation of Spontaneous Human and Murine PDAC Models

We generated spontaneous (without artificial immortalization) murine and human cell-based progression models of PDAC disease.

These models belonged to the same genetic background and represent different phenotypes/stages of PDAC disease. These were generated as follows:

(i) *Murine cell-based progression model of PDAC progression*. Mouse pancreatic progression model cell lines were generated from spontaneous tumors developed in *K-ras*^{G12D}/*Pdx*^{Cre}/*p16*$^{-/-}$ transgenic mice. Briefly, we euthanized two littermate mice of *K-ras*^{G12D} *Pdx*^{Cre} *p16*$^{-/-}$ genetic background. While one mouse exhibited the organ confined tumor, the other mouse exhibited relatively larger tumor with visible invasive nodules on body wall and liver. Tumor tissues were carefully removed and immediately transferred to culture medium (RPMI-1640 supplemented with 10% FBS.) followed by careful mincing under sterilized condition. Minced tumor tissues were grown as tumor explants as one explant per culture dish in soft-agar plated culture dishes. After 48 hours, explants were supplemented with fresh media and cultures were observed under microscope for cell propagation from explants. The noticeable observation was the growth of cells around the tumor explants after 1 week of seeding. The explants were removed when culture plates exhibited 100% confluence level of cells. Microscopic observation for the phenotype of cells suggested a heterogeneous mixture of fibroblast like cells (elongated) and epithelial cells (cobblestone). To generate the epithelial cell population, the heterogeneous mixture cells were allowed to undergo serial propagations for several weeks. With each week, the mixture of cells exhibited increased number of epithelial and decreased number of fibroblasts. At 12 weeks of serial propagation, homogenous epithelial cells from pancreatic tissues and metastatic nodules were obtained. Finally, three cells lines were generated from two littermates (same parents) and with similar genetic background *K-ras*^{G12D} *Pdx*^{Cre} *p16*$^{-/-}$. These were named as HI-Panc-L (derived from pancreatic tissue showing localized growth, small tumor, and no metastasis), HI-Panc-I (derived from invasive pancreatic tumor, showing body-wall metastasis invasion), and HI-Panc-M (derived from metastatic liver nodule).

(ii) *Human cell-based progression model of PDAC*: A human spontaneous model representing primary PDAC was developed from the pancreatic tumor of a (nonidentifiable) patient who did undergo the surgery at the Vanderbilt University (Nashville, TN). After surgery, tumor tissues were immediately transferred to the author's laboratory within 12 hours. Primary tumor cells were derived from human tumor using the same method as described for mouse tumor-derived cell models. The human model represents primary stage of PDAC disease and was named as UM-PDC1 (University of Minnesota-pancreatic ductal carcinoma) cells. UM-PDC1 cells were implanted in SCID mice to test the tumorigenic potential. UM-PDC1 tumors which exhibited tumors in SCID mice were harvested and used for deriving a second generation of UM-PDC cell line, which we named as UM-PDC2.

Tumor Xenograft Studies in Immunocompromised Mice

Murine cell models (HI-PancL, Hi-PancI, HI-PancM) were implanted (5×10^6 cells in 100 µl Matrigel/media; 50/50%) subcutaneously in athymic nude mice. Human cell model UMPDC was implanted (5×10^6 cells 100 µl Matrigel) subcutaneously in SCID mice. Animal were followed for tumor growth (in terms of volume), and tumor volume and weights were measured on a twice/week basis as described [11].

Chromosomal Arrangement and Karyotyping Assay

The human cell model karyotyping was performed by LeAnn Oseth at the Cytogenomics Center, University of Minnesota, whereas the murine cell model karyotyping was performed at the cytology core facility at the Roswell Park Cancer Center (Buffalo, NY). Briefly, three wells of a six-well plate of pancreatic tumor cells were exposed to colcemid treatment for 2 hours. Cells were harvested according to the standard cytogenetic protocol [12]. The metaphases (n=20) were completely analyzed at a 400-band level resolution.

Immunoblot Analysis, IHC, Transfections, Luciferase Reporter, Immunofluorescence Microscopy, and Chemoinvasion Assays

These were performed by using the methods as described previously [11,13]. Single-cell centrosome detection was performed as per the method provided in the supplementary tables and methods section.

Cilia Analysis

Cells were grown in four-well glass slides and, when confluent, incubated for 24 hours with DMEM without serum to stimulate ciliary growth [14,15]. Cells were then washed with PBS, fixed with iced methanol, permeabilized with 0.1% Triton X-100, and blocked with 0.1% Triton X100 and 10% normal goat serum in PBS. Cells were incubated overnight with antibodies against acetylated α-tubulin (1:200, Sigma-Aldrich) and γ-tubulin (1:500, Sigma-Aldrich) at 4°C followed by incubation for 1 hour with fluorescent secondary antibodies (1:200). Nuclei were stained with DAPI (Prolong Gold w/DAPI, Invitrogen), and ciliated cells were analyzed using confocal microscopy.

RNA Sequencing of Cell Models

We performed the RNA-seq analysis of hypoxic cell models. For this purpose, PDAC models were treated with cobalt chloride 100 µM for 24 hours. Cells were harvested and pellets were prepared in high-stringent and sanitized conditions (to avoid any exogenous RNA/DNA contamination). Cell pellets were transferred to the genomic center where high-quality RNA was extracted from these models. The libraries were prepared and analyzed on Illumina 2000 platform for sequencing. The initial data screening was performed by Bioinformatics core (Masonic cancer center, University of Minnesota). FPKM values were log transformed and mean centered prior to filtering for large changes. The RNA sequencing data were validated by quantitative real-time PCR analysis of top 50 genes (top 50 showing marked difference when compared localized tumor vs metastatic tumor) using murine (HIPanL, HIPancI, HI-PancM) and human (UM-PDC1, UM-PDC2) models. The primer information for QRT-PCR is provided in Supplementary Table 1. The RNA-seq data were submitted to GEO/NIH data base (Accession # GSE116635).

Gene Set Enrichment Analysis (GSEA)

The GSEA algorithm was applied to RNA-seq data for enrichment analysis. Log2 fold change was applied as the preranking metric ranking [16].

Association and Patient Survival Analysis

The comparison of ISX gene expression between pancreatic tumor tissue and normal tissues was done by an analysis using UALCAN (http://ualcan.path.uab.edu) and TCGA-PAAD clinical dataset of pancreatic carcinoma patients [17]. Pearson correlation coefficient was used to evaluate correlations. All patients were divided into two groups according to gene expression level in tumor tissue for survival analysis. The high-expression group consisted of patients in which gene expression levels were above the median value, and a low-expression group comprised the remaining patients. We stratified the analysis on the basis of associations between *ISX* gene expression and clinical features in OS such as gender, tumor stage, and age. The clinical features were adjusted in multivariate Cox proportion hazard regression analysis.

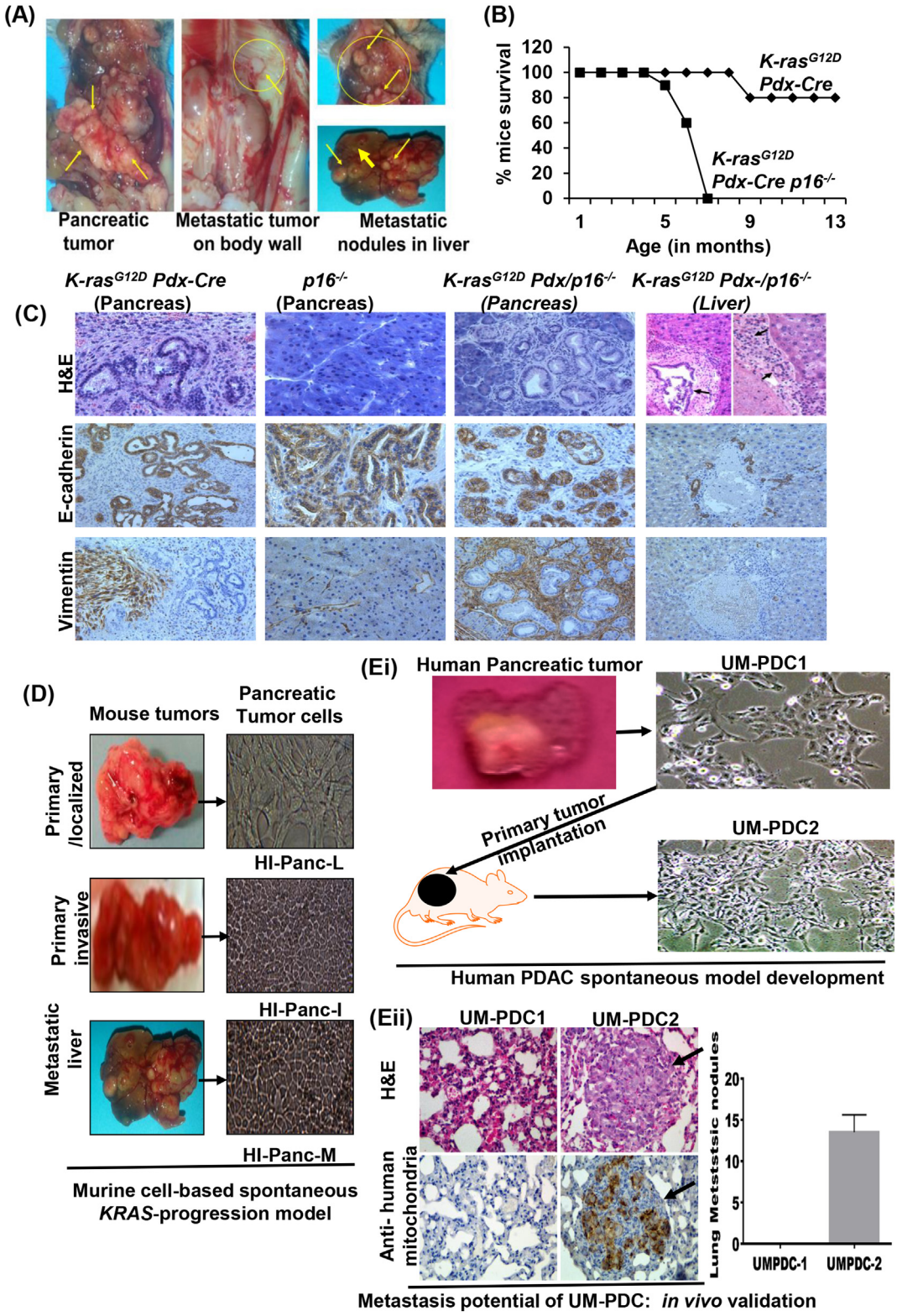

Figure 1. Transgenic *K-ras^{G12D} Pdx-^{Cre} p16$^{-/-}$* mice developed spontaneous localized, invasive, and metastatic pancreatic tumors. (A) Photographs showing the primary tumor and metastasis development in *K-ras^{G12D} Pdx^{Cre} p16$^{-/-}$* mice. (B) Line graph shows the comparison in the survival (as a function of age) of transgenic *K-ras^{G12D}/Pdx^{Cre} versus K-ras^{G12D} Pdx^{Cre} p16$^{-/-}$* mice. (C) Image showing the H&E and immunostaining for E-Cadherin and vimentin (phenotype markers) in primary and metastatic tumor (liver) resected from *K-ras^{G12D}/Pdx^{Cre,} INK4A/p16$^{-/-}$ and K-ras^{G12D}, Pdx^{Cre} p16$^{-/-}$* mice. Staining showed the pattern of E-Cadherin and Vimentin expression in spontaneous localized and metastatic pancreatic tumors in different transgenic mice. (D) Photographs showing the mouse tumors (from which cell lines HI-Panc-L, HI-Panc-I, and HI-PANC-M were generated). Light microscopy images showing morphology for HI-Panc-L HI-Panc-I and HI-Panc-M cells. (Ei) Photographs showing the human tumor specimen and scheme (by which UM-PDC1 and UM-PDC2 cell lines were generated). Light microscopy image showing morphology for human UMPDC cells. (Eii) H&E and IHC staining shows the metastatic potential of UM-PDC2 cell line *in vivo*. Paraffin sections of lungs were stained for H&E and IHC (for human mitochondrial protein) to determine the metastatic potential of UM-PDC1 and UM-PDC2 cells in a mouse tail vein/lung-metastasis model. Bar graph shows the quantification of metastatic nodules in lungs of mice.

Statistical Analysis

Student's *t* test for independent analysis was applied to evaluate differences between the normoxia and hypoxia cell conditions with respect to the growth, invasion and expression of proteins. A Kaplan-Meier survival analysis with the corresponding log-rank was used to measure the rate of mean tumor volume growth as a function of time. A *P* value of <.05 was considered to be statistically significant.

Result

Transgenic K-ras^{G12D}/Pdx^{Cre}/ p16$^{-/-}$ Mice

Transgenic *K-ras^{G12D}/Pdx^{-Cre}* or *p16$^{-/-}$* did not show malignant/metastatic PDAC formation; however, *K-ras^{G12D}/Pdx^{Cre}/p16$^{-/-}$* mice exhibited spontaneous pancreatic tumors, invasion of tumor in adjacent body wall, and liver metastasis (Figure 1*A*). The *K-ras^{G12D}/Pdx^{Cre}/p16$^{-/-}$* mice manifested multiple pancreatic tumor nodules that varied greatly in size (Figure 1*A*). These data are in agreement with findings of Bardeesy et al. and Aguirre et al. [10,18]. The overall survival in *K-ras^{G12D}/Pdx^{Cre}/p16$^{-/-}$* mice is significantly lower (<7 months) when compared to *K-ras^{G12D}/Pdx^{Cre}* mice (80% of mice lived up to 13 months) (Figure 1*B*). The majority of pancreatic tissues of K-*ras$^{G12D/}$Pdx^{Cre}* mice displayed high-grade PanIN formation and no ductal adenocarcinoma. On IHC analysis, majority of these tissues exhibited positive E-cadherin and negative vimentin staining (Figure 1*C*, panel 1). Nevertheless, some PanIN lesions were noted to be vimentin positive (Figure 1*C*, panel 1). H&E staining of the paraffin sections of *K-ras$^{G12D/}$Pdx^{Cre}/p16$^{-/-}$* pancreatic tumors confirmed that most nodules were ductal adenocarcinomas, ranging from well-differentiated to moderately differentiated histology (which were E-cadherin positive and vimentin negative) (Figure 1*C*, panel 3). However, regional mesenchymal features were also observed in some tumors which tested positive for vimentin (Figure 1*C*, panel 3). Histologically, most liver tumors manifested poorly differentiated morphology with sarcomatoid/mesenchymal features; however, some regions continued to exhibit ductal histology testing positive for E-cadherin (Figure 1*C*, panel 4). Autopsy did not find macroscopic lesions in the lung, kidney, stomach, spleen, and other abdominal organs or lymph nodes.

Characterization of Murine (HI-Panc-L, HI-Panc-I, HI-Panc-M) and Human (UM-PDC1 and UM-PDC2) Progression Models

The generation of HI-Panc and UM-PDC cell models is described in Materials and Methods. HI-Panc-I and HI-Panc-M cells display a typical cobblestone morphology, whereas HI-Panc-L cells though epithelial are elongated with a similarity to fibroblastic morphology (Figure 1*D*). Human primary and invasive tumor cell lines UM-PDC1 and UM-PDC2 are cobblestone shaped with clear demarcations of membrane and nucleus (Figure 1*Ei*).

Determining Metastatic Potential of Human UMPDC Models

A homogenous population of UM-PDC2 exhibits aggressive/invasive phenotype than UM-PDC1. We next determined the metastatic potential of human UM-PDC models in R2G2-immunocompromised mouse models. The metastasis potential of cells was determined by using a tail-vein injection in mouse model. R2G2 mice were injected with cells (UM-PDC1 and UM-PDC2), and mice were euthanized after 3 weeks. The gross metastasis in lungs and liver of mice was examined (using India ink method). The micrometastasis was determined by H&E and IHC analysis of tissues. The IHC analysis using human anti-mitochondrial protein marker antibody (that recognized human cells) confirmed the colonization of pancreatic tumors cells in the lung. The anti-mitochondrial protein marker was positive in UM-PDC2 metastatic nodules (Figure 1*Eii*). These data suggest that UM-PDC1 and UM-PDC2 represent a human spontaneous PDAC progression model (from same genetic background) and represent localized and metastatic stages of disease, respectively.

For the systematic characterization of models, we tested cells for the standard pancreatic markers α-Amylase, Pdx1, and PLA2GB by employing immunoblot analysis. All cell lines tested positive for pancreatic markers, and AsPC1 pancreatic cell line was used as positive control (Figure 2*Ai*). Anti-Pdx1 antibody is specific to mouse and therefore was not detected on immunoblot band for human cells (Figure 2, *Ai-ii*). We next evaluated the models for K-ras activity and measured K-ras-GTP levels in cells by using an active K-ras (K-ras-GTP) specific antibody. All cell models exhibited elevated levels of K-ras-GTP expression (Figure 2, *Aiii-iv*). Because AKT, NFκB, and MAPK are the well-known downstream targets of activated K-ras, we asked if a K-ras-regulatory mechanism is active in cell models [19]. Models exhibited the expression of active forms of AKT (phosphorylated) and NFκB-p65 (phosphorylated), and MAPK (ERK1/2) indicating an active K-ras signaling in these cells (Figure 2, *Bi-ii*). The PTEN (tumor suppressor), an antagonist of the phosphatidylinositol 3-kinase (PI3-K)/AKT signaling, has been reported to exhibit functional inactivation and loss of protein expression in PDAC cases [20]. Although testing positive in all murine cell models, the PTEN expression exhibited a gradual loss in human UMPDC progression models (Figure 2*Bii*), suggesting that progression of localized UM-PDC1 to metastatic UM-PDC2 is associated with the loss of PTEN. It has been reported earlier that PTEN loss is an important event during progression of PDAC from localized disease to metastasis (Figure 2*Bii*). VEGF is required for tumor cells to sustain their growth by generating new blood vessels around tumors [21]. VEGF expression was detectable in invasive and metastatic murine models (Figure 2*Bii*). Next, we measured the doubling time, 3D clonogenicity, and invasiveness potential of cells by using Trypan blue dye exclusion, chemoinvasion, and soft-agar clonogenicity assays; data showed that UMPDC-1, UM-PDC2, HI-Panc-L, HI-Panc-I, and HI-Panc-M cells exhibit a doubling time of 48, 36, 48, 36, and 24 hours, respectively (Figure 2*Ci*). We tested the clonogenic potential of cell lines by soft-agar colony formation assay. In a 14-day duration, all cell lines exhibited clonogenic potential in the order of HI-Panc-M >HI-Panc-I >HI-Panc-L and UM-PDC2>UM-PDC1 (Figure 2*Cii*). HI-PancM cells exhibited higher invasiveness potential than HI-Panci, whereas HI-PancL exhibited none (Figure 2*Ciii*). Similarly, UM-PDC2 exhibited more invasive potential than UM-PDC2 (Figure 2*Ciii* & Supplementary Figure 2*Ai*). Next, we determined the tumorigenic potential of cell lines in immunocompromised mice model. For testing the tumorigenicity of murine models, tumor cells were subcutaneously implanted in the right flank of female athymic nude mice maintained under sterilized conditions. Animals were followed for weight, tumor growth, and general health on daily basis as per IACUC guidelines. We also tested the tumorigenicity of human UM-PDC model in SCID mouse model. HI-Panc-I and HI-Panc-M cells exhibited rapid tumor growth than HI-Panc-L cells (Figure 2*Di*). Human UM-PDC1 and UM-PDC2 cell models formed large-sized tumors within 4-6 weeks postimplantation (Figure 2*Di*). Notably, the initial rate of tumor growth of HI-

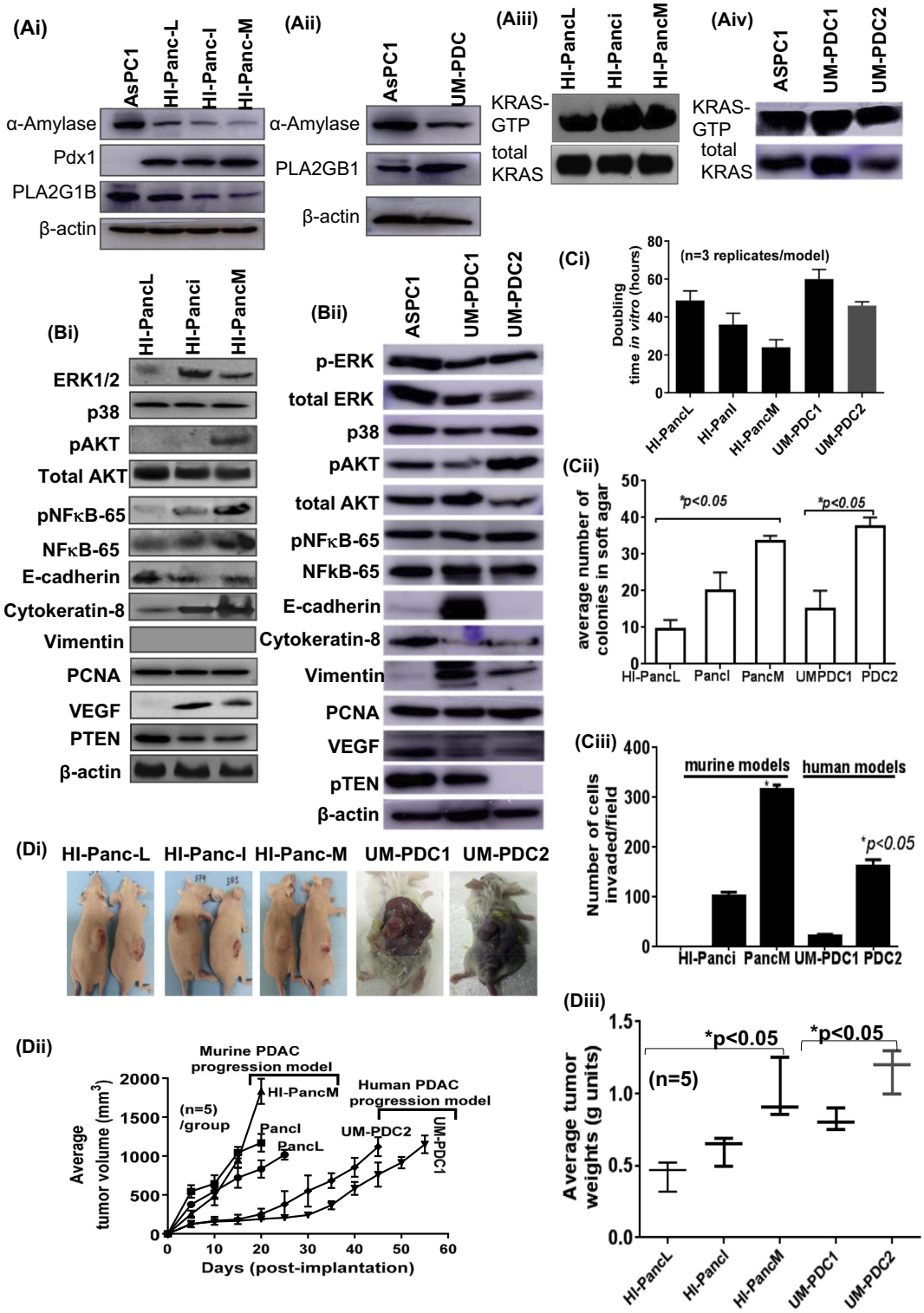

Figure 2. Characterization of HI-PancL, HI-PancI, HI-PancM and UM-PDC models. (A) Immunoblot images showing the expression of (Ai-Aii) pancreatic markers (α-Amylase, Pdx1, and PLA2G1B) and (Aiii-Aiv) K-ras activity status in murine (HI-Panc-L, HI-Panc-I, & HI-Panc-M) and human PDAC models (UM-PDC). A known PDAC cell line AsPC1 was used as a reference control. (B) Immunoblot images showing the expression of (Bi-Bii) downstream targets of K-ras pathway ($ERK^{1/2}$, p38, pAkt, total Akt, pNFκB-p65, total NFκB-p65, VEGF), epithelial markers (E-Cadherin, Cytokeratin-8), and proliferation marker (PCNA) in murine and human PDAC models. (C) Histograms showing the (Ci) cell doubling time (in hour units) $n=3$ replicates/model; (Cii) 3-dimensional clonogenic potential of HI-Panc-L, HI-Panc-I, HI-Panc-M, and UM-PDC models; (Ciii) invasiveness potential; and (D) the tumorigenic potential of cell models as xenografts in mouse models (Di) photographs showing intact tumors on athymic nude (for murine models) and SCID (for human model) mice. (Dii) Line graph showing the growth of tumors in mice as a function of time to average tumor volume ($n=5$). (Diii) Graph showing the average weight of tumors formed by cell models when implanted in immunocompromised mice ($n=5$).

Panc-I and HI-Panc-L was almost similar; however, HI-Panc-I group progressed faster than HI-Panc-L after 10 days (Figure 2*Dii*). Animals exhibiting tumor volume of >1000 mm^3 were sacrificed. The harvested tumors were measured for weight. HI-Panc-M and UM-PDC2 cell-derived tumors showed highest volume followed by HI-Panc-I and HI-Panc-L (Figure 2*Diii*). Taken together, these data establish that all the cell line models are highly tumorigenic when implanted in immunocompromised animals.

Status of Genomic Stability of Pancreatic Cells During Progressive Stages of PDAC

Genetic instability has long been considered an integral component of human neoplasia, and solid tumors are nearly all genetically unstable [22]. Aberrations in the number and structure of chromosomes are a hallmark of cells derived from solid tumors [22]. These aberrations include gross chromosomal rearrangements (including translocations, large deletions, or inversions), gene copy number variations (due to defective DNA replication or repair), and anomalous chromosome number (due to defective segregation between daughter cells during cell division) [19 and references therein]. We determined the chromosomal arrangement of murine (Hi-Panc-L, HI-Panc-I, and HI-Panc-M) and human (UM-PDC1 and UM-PDC2) models by performing karyotype analysis on 20 metaphase chromosomes using SKY and conventional G-banding techniques. These analyses revealed an abnormal karyotype for all cell lines with a modal chromosome number of 40, 80, 81, 72, and 72 for Hi-Panc-L, HI-Panc-I, HI-PancM, UMP-DC1, and UM-PDC2, respectively (Supplementary Table 2). In addition to having an abnormal number of chromosomes, sample HI-Panc-L contains a translocation der(16)t(6:16) which consists of a very small portion of chromosome 6 at the distal end of chromosome 16 (Figure 3, *Ai-iii*). HI-Panc-M cells were shown to contain a deleted copy of chromosome 14. The HI-Panc-I cells exhibited translocations in only one cell analyzed (Figure 3*Aii*). There was a der(6)t(6:7) translocation which is made up of equal portions of chromosome 6 and chromosome 7 as well as a robertsonian translocation rbt(11:11). HI-Panc-M did not exhibit any chromosomal rearrangement (Figure 3*Aiii*).

All the 20 of the metaphase cells analyzed for UM-PDC1 and UM-PDC2 had a hypertriploid karyotype with 72 chromosomes and multiple numerical and structural abnormalities. Relative to a pure triploid karyotype that would have three copies of chromosomes 1 through 22, there was a loss of one copy each of chromosomes 13 and 16, one extra copy of chromosomes 5, 6, 14, and 20, and two extra copies of 8 (Figure 3*Aiv*). Included among the abnormalities were multiple isochromosomes: two for the short arms of chromosome 5, two each for the long arms of chromosomes 8 and 9, and one for the short arms of chromosome 18. Most notable were the presence of two isochromosomes for 8q, yielding a total of 7 copies of this long arm. Other structural abnormalities included additional material of unknown origin added to the long arms of chromosomes 4, 9, 11, and 12 and to the short arms of chromosomes 14 and 18, and deletions within two of the four copies of chromosome 20. Each of these cells had two X chromosomes present, indicating a loss of a Y (Figure 3*Aiv*). UMDPC2 differs from UMPDC-1 in having long arm of a chromosome 5 attached to the long arm of chromosome 4; material from the long arm of a chromosome 13 attached to the long arm of one chromosome 9; material from chromosomes X and 20 attached to the long arms of the two isochromosome 9s; abnormal chromosomes 11 and 12, which SKY identified to be composed entirely of 11 and 12, respectively, formed by duplications and/or deletions in the long arm of each chromosome; material from the long arm of a chromosome 16 attached to the long arm of chromosome 14; an isochromosome 14 with material from the long arm of a chromosome 16 attached at both ends; material from the long arm of a chromosome 12 attached to the short arm of one chromosome 18; deletion within two of the four copies of chromosome 20 (Figure 3*Av*).

Defects in chromosome segregation during mitosis contribute to genetic instability during tumorigenesis [23]. One of the known causes of chromosome missegregation in dividing neoplastic cells is the abnormal centrosome number that causes the formation of transient multipolar mitotic spindles [24–27]. Structural and functional centrosome abnormalities are reported in human PDAC [24]. We measured number of centrosomes (in the dividing cells) by performing immunofluorescence-based microscopy analysis of single cells. As represented by microscopy image (Figure 3, *Bi-ii*) and histogram (Figure 3*Biv*), we show that both the localized and invasive PDAC cells have an increase in the number of centrosomes/cell. These data suggest that chromosome mis-segregation driven by the presence of supernumenary centrosomes/spindle poles contributes to a silent phenotype (chromosomally instable cells) that reflects the aggressive disease. Interestingly, the metastatic cells (Hi-Panc-M) show a return to the normal centrosome/cell number (Figure 3, *Bi-ii*). This suggests the intriguing possibility that during clonal selection for the metastatic cells, the abnormal centrosome duplication phenotype becomes suppressed. The result is a highly aggressive yet chromosomally stable clone of tumor cells. We next determined the number of centrosomes (in the dividing cells) in UM-PDC1 and UM-PDC2 by performing immunofluorescence-based microscopy analysis of single cells. As represented by microscopy image (Figure 3*Biii*) and histogram (Figure 3*Bv*), we show that both the invasive/metastatic UM-PDC2 have an increase in the number of centrosomes/cell. We also observed the gross colocalization of α-tubulin/γ-tubulin and α-tubulin/E-cadherin in all cell models (Supplementary Figure 2*Aii*).

Phosphorylation is a widely recognized mechanism of regulating chromosome biorientation, tension sensing, and chromosome movement during mitosis [28]. Aurora Kinase A (serine/threonine kinase) is reported to be involved in controlling chromatid segregation in cells [29]. Histone H2AX (a mammalian histone H2A variant) is reported to promote DNA double-strand break repair and undergoes rapid phosphorylation by kinases to form γ-H2AX over large chromatin domains surrounding DNA double-strand breaks [30]. Therefore, Aurora Kinase A and H2AX are used as surrogate biomarkers for the genomic stability of cells. We determined the Aurora Kinase A and H2AX expression levels and localization in cell lines by using confocal microscopy. The fluorescence-immunostaining data show Aurora kinase A localization at outer membrane of dividing cells and H2AX in nuclei of dividing cells (Figure 3*C*). Notably, the elevated levels of H2AX observed in HI-Panc-M (metastatic cells) suggest that cells at metastatic pancreatic tumor cells undergo a significant DNA damage.

Several studies show that centrosome decides the fate of cells (for phenotype) by affecting the assembly of primary cilia in cells [31]. Primary cilia are multisensory organelles expressed in almost every epithelial cell of the body [32]. Recent studies show that the loss of primary cilia in the tumor cells is a common occurrence in solid tumors such as breast, prostate, and kidney [33]. We characterized the expression of cilia in our cell models. Acetylated-α-tubulin is considered a

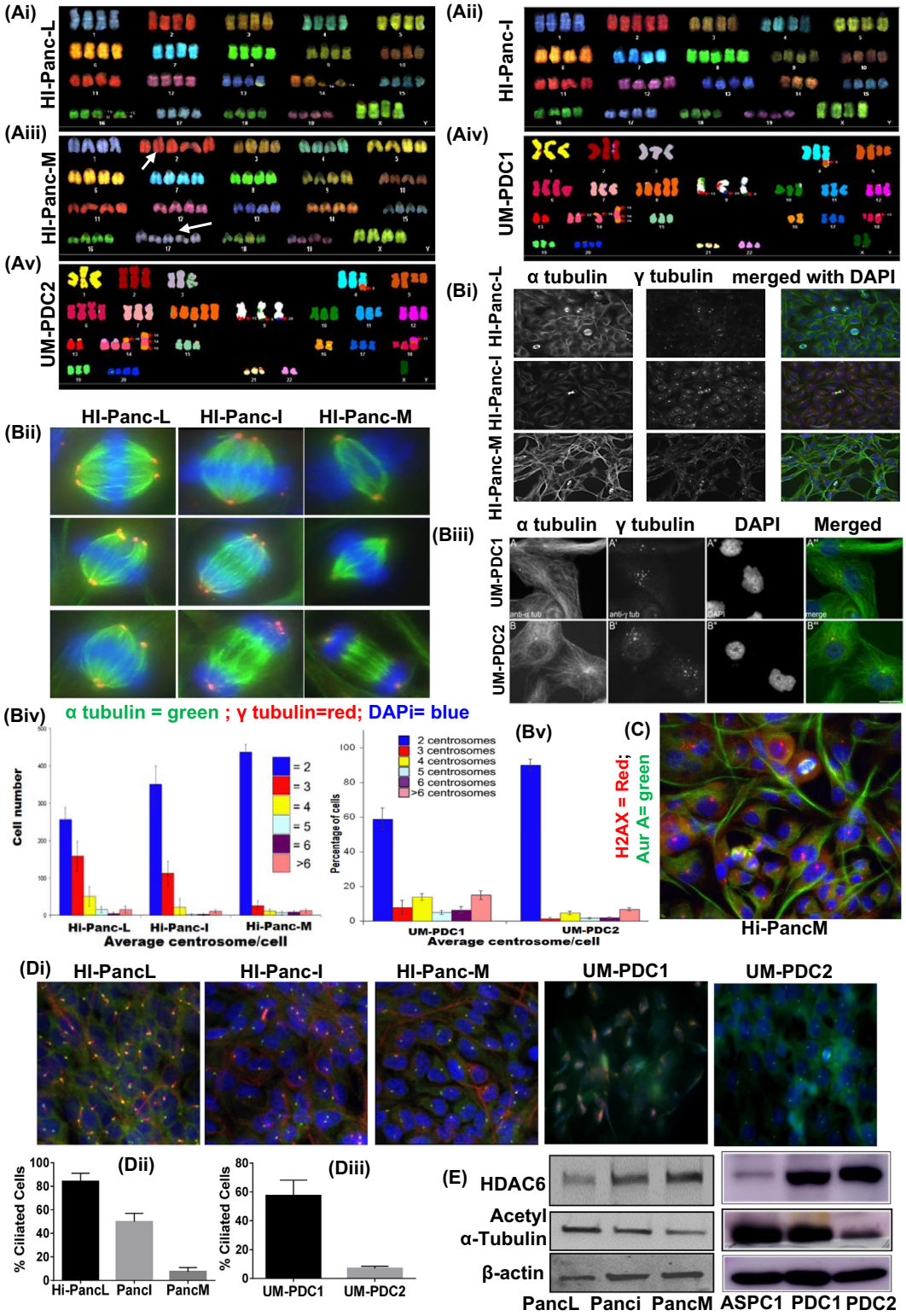

Figure 3. Chromosomal distribution and genomic stability (centrosome segregation & ciliagenesis) during progressive stages of PDAC. (A) Photographs showing the spectral karyotyping analysis of (Ai-iii) murine and (Aiv-v) human models. Images show chromosomal structure, aberrations, and translocations. (B) The centrosome segregation during division of cell models. Photomicrographs showing centrosome segregation during division by gross colocalization of α-tubulin/γ-tubulin in (Bi) Hl-Panc and (Bii) UM-PDC cell models using immunofluorescence microscopy. (Biii) Photographs show the single-cell captured images of centrosomes (immunostained with α-tubulin and γ-tubulin) by using fluorescence microscope. (Biv) Histograms showing the average number of centrosomes/cell in Hl-PANC and UM-PDAC cell models. The number of centrosomes/cell was counted from maximal projection images of γ-tubulin-labelled cells. (C) Photomicrographs showing the colocalization of Aurora kinase/H2AX in metastatic models using immunofluorescence microscopy. (D) Primary cilia status in murine and human PDAC cell models. (Di) Photomicrographs showing acetylated-α-tubulin (marker of cilia) positive cells as determined by confocal microscopy. (Dii-iii) Histograms showing the quantification of the acetylated-α-tubulin (marker of cilia) positive cells. of cilia) positive cells as determined by confocal microscopy. (E) Immunoblot image showing the expression of acetylated-α-tubulin and HDAC6 in murine and human cell models. The β-actin was used as the loading control in immunoblot analysis.

marker of primary cilium in the cells [34]. We used confocal microscopy and Western blot analysis to determine acetylated-α-tubulin status in cell models. As shown in the Figure 3*Di*, primary cilia expression significantly decreased with increasing disease stage of PDAC models in an order of UM-PDC1>UM-PDC2 and HIPancL>HIPanci>HIPancM (Figure 3, *Dii-iii*). Recent studies showed that the loss of primary cilia in neoplastic

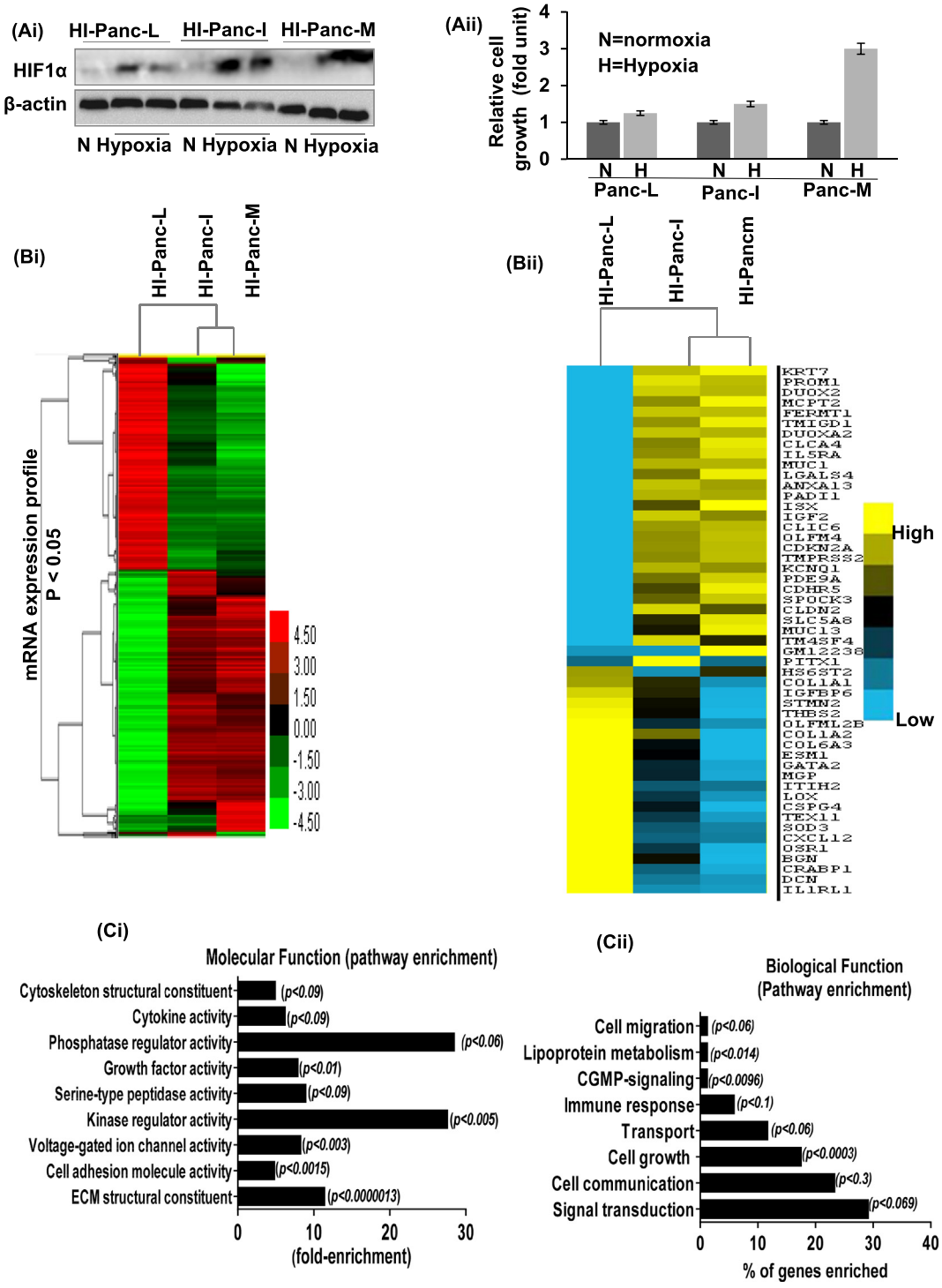

Figure 4. Status of the genetic landscape of tumor cells growing under hypoxic conditions during progression of PDAC disease. (Ai) immunoblot shows the expression of HIF1α (marker of Hypoxia) following induction of hypoxia by Cocl2 treatment. (Aii) Bar graphs shows the relative cell growth in fold units grown in hypoxia and normoxia. (B) RNA-seq analysis of cell models grown under hypoxia conditions. (Bi) Hierarchical clustering of HI-Panc-L, HI-Panc-I, and HI-Panc-M cell models based on gene expression values from RNA-seq data. Heat map represent fold change expression of differentially regulated genes with threshold of ≥2 fold change, $P < .05$, and FDR value < 1. The red color in the heat map represents fold change >1.5 (upregulated), and green color represents fold change <−1.5 (downregulated). (Bii) Heat map of top 50 genes showing the significant changes (when compared during disease progression). (C) Cells grown under hypoxia were evaluated for genetic changes using RNA sequencing. Histograms show the hypoxia-responsive (Ci) molecular functions and (Cii) biological function changes in PDAC models as determined by Inguinity pathway enrichment analysis of RNA-seq data.

cells as exemplified by the deacetylation of α-tubulin (the structural component of the ciliary axoneme) could be mediated by histone deacetylase 6 (HDAC6), a cytoplasmic deacetylase [31]. The deacetylation of α-tubulin induces destabilization of the axoneme and ciliary resorption [35]. By employing immunoblot analysis, we determined the status of HDAC6 expression in progression cell model and found that the HDAC6 expression increased with the aggressiveness of the PDAC stage in an order of UM-PDC1< UM-PDC2 and HI-Panc-L HI-Panc-I HI-Panc-M (Figure 3*E*). When compared, the expression of HDAC6 was observed to inversely correlate to the levels of acetylated-α-tubulin, suggesting role of HDAC6 in the loss of primary cilia during PDAC development (Figure 3*E*).

Identifying Hypoxia-Driven Genetic Changes During Progression of PDAC

Hypoxia is a prominent feature in the microenvironment of pancreatic tumors [36]. Therefore, we compared the growth rate of HI-Panc-L, HI-Panc-I, and HI-Panc-M cells upon treatment with $CoCl_2$, which is known to induce HIF1α mimicking a hypoxic state in cancer cells (Figure 4*Ai*). Aggressive cell proliferation was observed when HI-Panc cell models were grown under hypoxic condition, and HI-Panc-M model registered the highest growth among all models under hypoxia (Figure 4*Aii*). We repeated the studies using a hypoxia chamber, and the data were similar to CoCl2-induced hypoxia (not shown).

To identify key genes underlying the progression of PDAC from localized disease to a metastatic form, we performed whole transcriptome RNA sequencing analysis of murine cell models through paired-end deep sequencing. We performed Kal's *Z*-test of FPKM values for measuring comparative gene expression profile. By applying stringent statistical threshold (> or = to 1.5 FC, $P < .05$), we identified genes differentially expressed in models representative of three different stages of PDAC. Unsupervised hierarchical clustering showed that the HI-Panc-I (invasive) and HI-Panc-M (metastatic) cell lines exhibited comparable expression profile and clustered well separated from HI-Panc-L (localized) cells (Figure 4*Bi*). Next, we selected a set of 50 genes that could be tested as marker specific for PDAC progression on the basis of expression FC (higher fold change), level of significance (lower p value), and enrichment in pathways (Figure 4*Bii*). We next conducted the pathway enrichment (ingenuity pathway) analysis of RNA-seq data of hypoxic HI-Panc models using a Qiagen IPA software. The molecular and biological function analysis showed an enrichment in the signal transduction and cell communication pathways in hypoxic environment of tumor cells (Figure 4, *Ci-iv*). For the validity in biological replicates, a quantitative qPCR validation was performed for randomly selected genes in murine and human cell models grown under hypoxia. We observed significant changes in the expression of *ISX, CLCA4, SLC5A8, TEX11, CRABP1, CLC12*, and *BGN1* genes under hypoxic conditions during PDAC progression (Figure 5, *Ai-iv*).

Pancreas plays a significant role in metabolism and metabolic diseases in humans. Patients with metabolic diseases have been reported to be at high risk of developing PDAC [37]. Notably, among the all members of the hypoxia-responsive gene set (*ISX, CLCA4, SLC5A8, TEX11, CRABP1, CLC12*, and *BGN1*), Intestinal Specific homeobox protein *(ISX)* is the prominant factor that is reported to be involved in metabolic activities and disorders in humans. ISX has been reported to regulate the metabolic flux and immune system [38]. This generated an interest to study the relevance and function of *ISX* in PDAC disease. To extract additional information from the whole transcriptome changes occurring during the progression of localized PDAC to metastatic PDAC, the complete gene expression dataset was submitted to GSEA with respect to *ISX*-positive PDAC [16,39]. The *ISX* oncogene was found to exhibit a positive enrichment score in RNA-seq data of hypoxic-tumor cell models. Critical pathways for the *ISX*-relevant gene sets obtained were identified to be associated with mitosis, apoptosis, oncogenes, tumor suppressor expression, inflammation, nonclassical M2-activated macrophages, transcription, and RNA polymerase II (RNA pol II) transcription factor activity. The M2-activated macrophages gene set showed negative enrichment (enrichment score −0.46) in *ISX*-positive tumors (*ISX* rank metric score = 2.749, running ES *ISX* = 0.0429, FDR *q* value = 0.00614) (Figure 5*Aiii*). This indicates that hypoxic pancreatic tumor cells of advanced disease stage have an enrichment of M2-polarized macrophages gene set. Notably, M2 polarized macrophages are known to play role during tumor progression. Further, *RNA pol II* gene set showed negative enrichment (enrichment score −0.36042485) in *ISX*-positive tumors (*ISX* rank metric score = 2.749, FDR *q* value ≤ 0.001) (Figure 5*Ci*). *RNA pol II* gene set contains a number of tumor suppressor genes such as *PITX1, EGR1, EGR2, HEY1, BAFT2 KLF12,* and *GATA2* which we found to have a negative enrichment in metastatic cell model (Hi-Pancm) (Figure 5*Cii*). We postulate that the reason *ISX* oncogene might be associated to the downregulation of *RNA-pol II*–enriched tumor suppressor gene set.

ISX Expression in PDAC Models

The RNA sequencing and validation by qRT-PCR data showed that *ISX* exhibits a marked increase in its expression during the PDAC progression (Figure 4). *ISX* belongs to a homeo domains containing transcription factors family which is associated with inflammation, cell growth, differentiation, and morphogenesis [40,41]. Using immunoblotting, we determined the *ISX* protein levels in murine Hi-PancM and human UM-PDC cell models. ISX protein levels were to found to be higher in metastatic (HI-PancM, ASPC1) than in primary PDAC cells (PancL, UMPDC1) (Figure 6*A*). We next performed IHC analysis and confirmed the presence of ISX protein in PDAC tumors (Figure 6*B*). When compared, the adenocarcinoma tumors exhibited higher levels of ISX levels than in normal pancreas. Notably, ISX protein was also observed in hyperplasia regions (HG-PanIN regions) of NAT (normal-associated tumors) specimens.

Association Analysis: TCGA-PAAD Clinical Study in Patients

We performed the data mining to identify the status of *ISX* expression in large cohort of PDAC patients using oncomine data sets. Using the oncomine database [42], we analyzed TCGA data 2013 (case *n*=100) and found that PDAC cases exhibited higher copy number of *ISX* than other types of pancreatic diseases in humans (Figure 6*Ci*). We next determined whether *ISX* expression accurately and independently determines survival of PDAC patients taking into account tumor grade, sex, and age. This was performed on the PAAD-TCGA dataset. The patient specimens were distributed on the basis of expression level (*ISX*-low/medium, ISX-high) and gender (male and female) subgroups. The high- and low-expression groups were formed based on the cutoff median level of *ISX* expression. We compared approximately equal size of male (*n*=20) and female (*n*=25) patients exhibiting high expression of ISX. The Kaplan-Meier analysis of overall survival of TCGA-PAAD data set showed that *ISX*-high female patients (*n*=25) exhibit a significant ($P = .034$) and negative correlation to

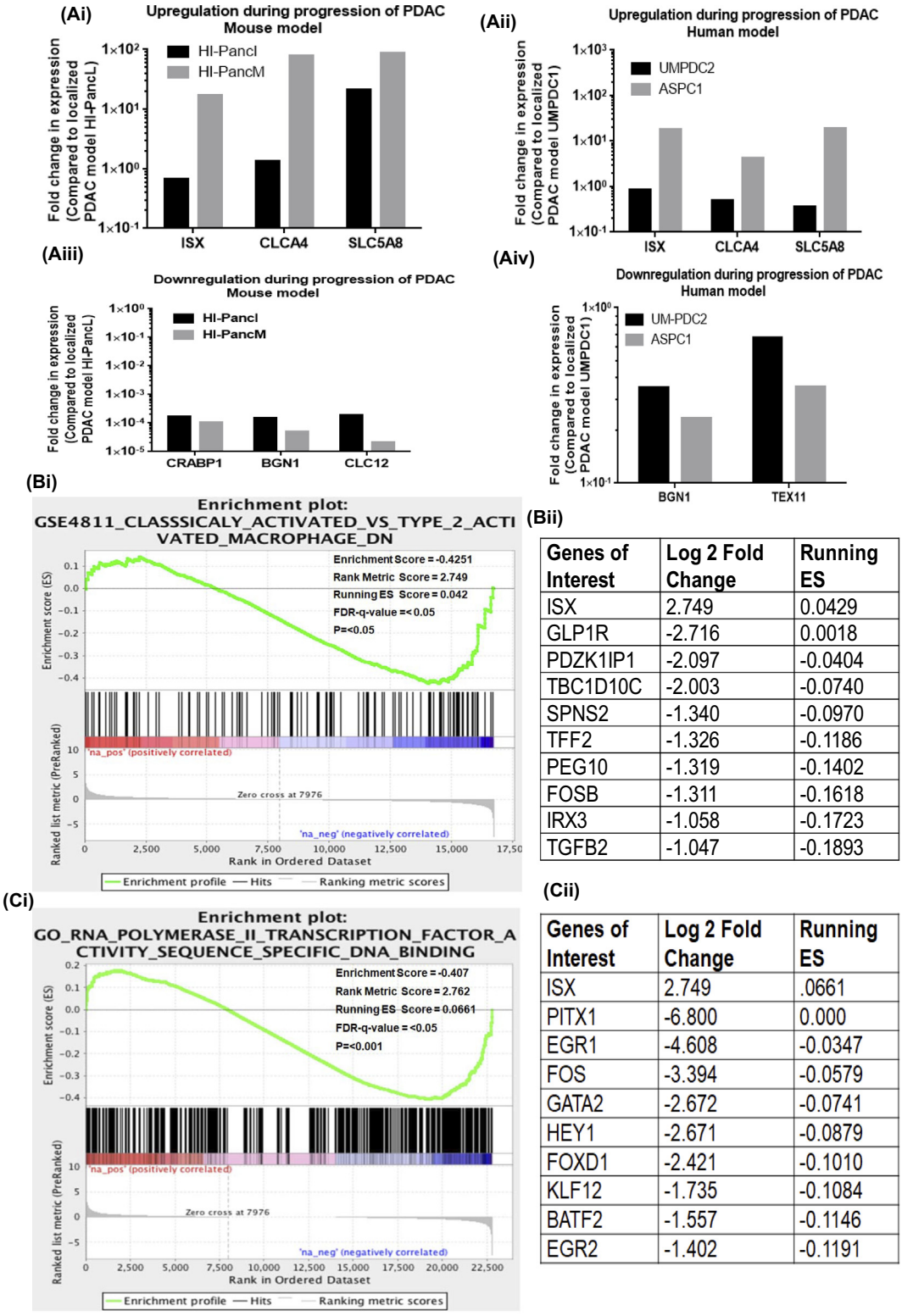

Genes of Interest	Log 2 Fold Change	Running ES
ISX	2.749	0.0429
GLP1R	-2.716	0.0018
PDZK1IP1	-2.097	-0.0404
TBC1D10C	-2.003	-0.0740
SPNS2	-1.340	-0.0970
TFF2	-1.326	-0.1186
PEG10	-1.319	-0.1402
FOSB	-1.311	-0.1618
IRX3	-1.058	-0.1723
TGFB2	-1.047	-0.1893

Genes of Interest	Log 2 Fold Change	Running ES
ISX	2.749	.0661
PITX1	-6.800	0.000
EGR1	-4.608	-0.0347
FOS	-3.394	-0.0579
GATA2	-2.672	-0.0741
HEY1	-2.671	-0.0879
FOXD1	-2.421	-0.1010
KLF12	-1.735	-0.1084
BATF2	-1.557	-0.1146
EGR2	-1.402	-0.1191

Figure 5. The pathway and GSEA analysis of tumor cells growing under hypoxic conditions during progression of PDAC disease. (A-Aiii) Bar graphs showing the qRT-PCR validation of five genes (*ISX, CLCA4, SLC5A8, BGN1, TEX11*) selected from RNA-seq data analysis. (Bi-ii) GSEA enrichment plot of HI-PANC cell model showing the negative enrichment of tumor suppressor genes with *ISX* gene. The top panel of the figure plots the enrichment scores (ES) for each gene, whereas the bottom panel of the plot shows the value of the ranking metric moving down the list of ranked genes. (Bii) The table enumerates the top tumor suppressor genes showing negative enrichment with *ISX* gene. (Ci-ii**)** GSEA enrichment plot of HI-PANC cell model showing the negative enrichment of negative regulators of M2 macrophages genes with *ISX* gene. (Cii) The table enumerates the top negative regulators of M2 macrophages gene with *ISX* gene.

the survival than male counterparts (n=20) (Figure 6*Cii*). We found that female patients harboring high *ISX* expression exhibit the least survival.

We also compared relevance of survival in low–ISX expression to high-expression patients. We compared low-expression (n=55) and high-expression (n=25) *ISX* in survival of female patients. When plotted for survival, the difference looks apparent, i.e., low–*ISX* expression group showed more survival (>2000 days) than high–*ISX* expression group (<500 days); however, the statistical P value (P=.08) is lower than our high stringent cutoff value of P<.05 for statistical significance. Therefore, this data set was deemed as insufficient, which could be due to a large difference in patient numbers between the two groups. We suggest that a comparative study of low *ISX* expression to high *ISX* expression with reference to survival should be conducted in a large cohort of approximately

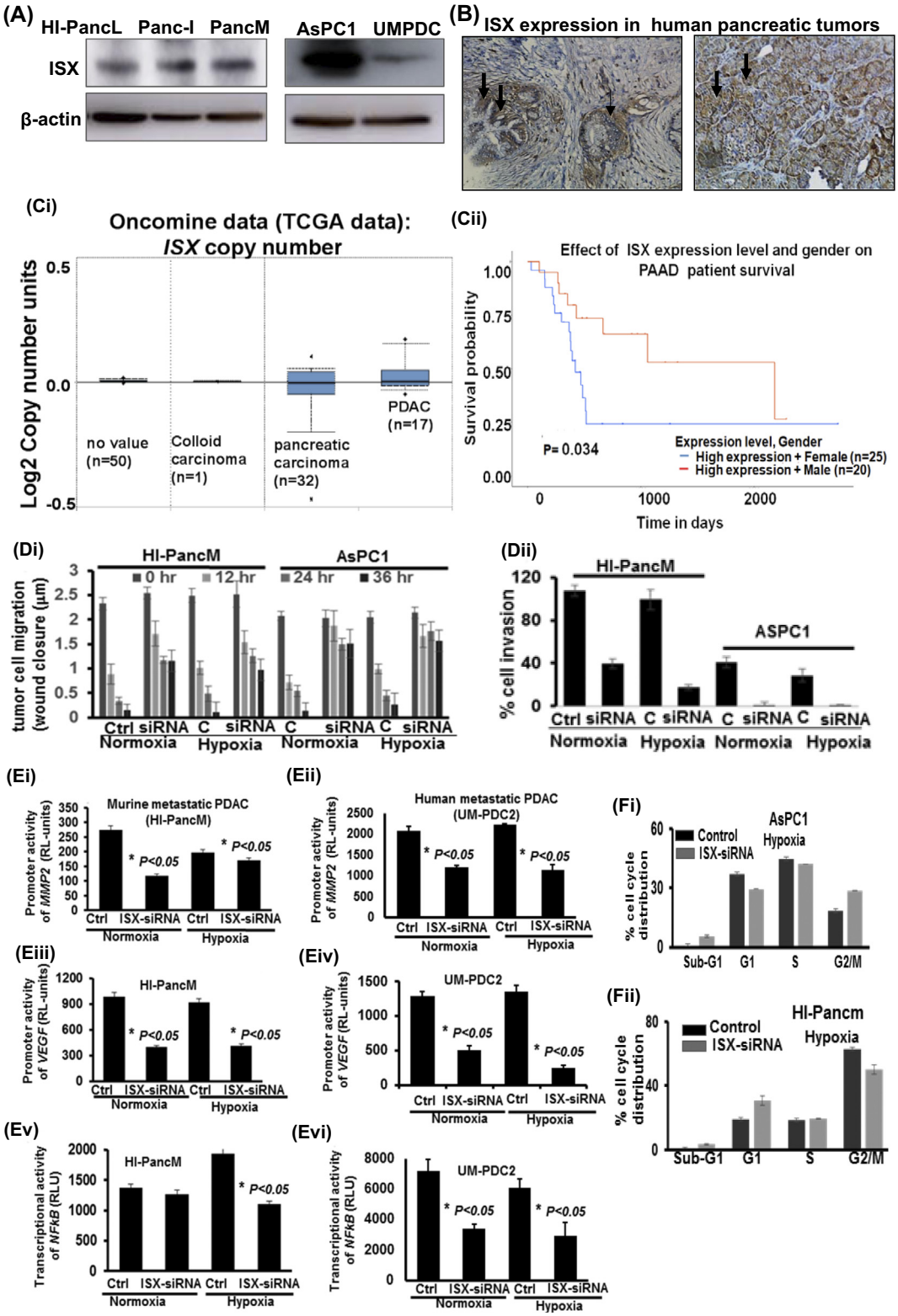

equal number for patients (low ISX expression vs high ISX expression).

Relevance of ISX in PDAC Metastasis

Metastasis is a complex process and includes steps such as loosening of tumor cells from the primary tumor, migration of tumor cells through the tumor tissue, crossing of endothelium membrane, intravasation/extravasation of tumor cells through blood vessels, traveling to distant sites, and homing at distant sites/metastatic sites to form secondary tumors. Migration of tumor cells is an important step for the metastasis multistep process. We determined the relevance of ISX on the migratory potential of tumor cells grown under normoxia and hypoxia conditions employing using a scratch wound-healing assay as described previously [43]. For this purpose, *ISX* expression was suppressed by siRNA in HI-Panc-M UM-PDC-2 and AsPC1 cells grown under hypoxia conditions. We evaluated the impact of *ISX*-suppression on the i) migration and ii) invasiveness potential of PDAC cells by using scratch wound-healing and chemoinvasion assays, respectively. The gap generated (due to scratch) in the center of the cell monolayer is akin to a wound which would be filled by migratory cells and the wound closure was measured at different time points (12, 24, and 36 hours postscratch) under microscope. *ISX* suppression was observed to significantly ($P<.05$) delay the migration of tumor cells under normoxia as well as hypoxia conditions; however, the effect of *ISX* suppression was noted remarkable in hypoxic cells (Figure 6*Di* & Supplementary Figure 2*B*). We next determined the relevance of *ISX* in the invasiveness potential of metastatic cells by employing a chemoinvasion assay and observed that *ISX* suppression causes a significant ($P<.05$) inhibition (>90%) in the invasiveness potential of human and murine metastatic cells (Figure 6, *Di-ii* & Supplementary Figure 2*C*).

Degradation of extracellular matrix in the host tissues is required by tumor cells for metastasis, and proteases (such as matrix metalloproteases; MMP) are critical for this process. MMP2 plays a role in the metastasis of pancreatic tumor cells in human patients [44,45]. By employing a luciferase reporter assay, we determined the activation of *MMP2* gene and observed that suppression of *ISX* significantly ($P<.05$) decreases the promoter activity of *MMP2* in human and murine metastatic PDAC cells (Figure 6, *Ei-ii*). These data were also validated in known metastatic cell model ASPC1 (Supplementary Figure 2, *Di-iii*).

VEGF activation is reported to be correlated to the metastasis and poor prognosis in PDAC patients [46]. We observed that the suppression of *ISX* causes a significant ($P<.05$) decrease in the *VEGF* promoter activity in human and murine metastatic PDAC cell models (Figure 6, *Eii-iv*). *MMP2* and *VEGF* activation is reported to be associated with the activation of *NFκB,* and the role of NFκB in the progression of PDAC is well established [47]. We next evaluated if a possible link between *ISX* and *NFκB* activity exists in PDAC models. Notably, we found that the suppression of *ISX* causes a significant inhibition in the transcriptional activity of *NFκB* in cell human and murine metastatic PDAC cell models grown under either conditions of normoxia and hypoxia (Figure 6, *Ev-vi*). Taken together, our data suggest a positive association between ISX and the activation of NFκB/MMP2/VEGF molecular network in PDAC cells. These data were also validated in ASPC1 cells (Supplementary Figure 2, *Di-iii*). Finally, we investigated if ISX status has a bearing on the proliferation and cell cycle of metastatic cells using a flow cytometry (FACS) assay. Under normoxia conditions, *ISX* suppression did not cause significant change in cell cycle profile (G1, G2 phases); however, it caused an increase in sub-G1 population of human cells (Supplementary Figure 3, *A-B*). Notably, suppression of *ISX* was observed to cause an increase in Sub-G0/G1 and G2/M population of cells growing under hypoxia compared to control cells (Figure 6, *Fi-ii* and Supplementary Figure 3, *Ci-ii*). To summarize, these data identify ISX molecule playing a key role in the hypoxia-induced metastasis process in PDAC disease.

Discussion

The activating point mutation of the *K-ras* oncogene on codon-12 accounts for 70%-95% of PDAC cases and 71%-75% of pancreatic cancer specimens [19,48]. The K-ras oncogene encodes for a small GTPase that acts as a molecular switch by coupling cell membrane growth factor receptors to intracellular signaling pathways to control various cellular processes. The point mutation of K-ras impairs intrinsic GTPase activity of RAS and prevents conversion of GTP (active) to GDP (inactive). P21 RAS is thus permanently bound to GTP and activates downstream signaling pathways, such as PI3K/AKT/mTOR, RAF, or MEK/ERK [19,48]. $K\text{-}ras^{G12D}/Pdx^{Cre}$ mice develop only the precursor PanIN lesions. An important observation in this study is that pancreatic adenocarcinoma in $K\text{-}ras^{G12D}/Pdx^{Cre}/p16^{-/-}$ mice seemed to be more aggressive than the observations reported by of Aguirre et al. [10]. This is supported by our findings of I) overt liver metastatic tumors, II) sarcomas in the liver, and III) vimentin-positive sarcomas in pancreatic tissue in $K\text{-}ras^{G12D}/Pdx^{Cre}/p16^{-/-}$ mouse model. Nevertheless, the majority of tumors formed were identified to be PDAC. We surmise that the pancreatic lesions are metastatic from the pancreas as well, which indicates that these stromal-originated pancreatic sarcomas are also very malignant. The noticeable observation in this study is that we generated cell models (HIPancl, HIPanci, HIPancm) from $K\text{-}ras^{G12D}/Pdx^{Cre}/p16^{-/-}$ mouse model which exhibits various different phenotypes and three different

Figure 6. ISX as a progression biomarker and regulator of metastasis process in PDAC disease.(A) Immunoblot image showing the expression of ISX protein in murine and human cell models. The β-actin was used as the loading control in immunoblot analysis. (B) Photomicrograph showing the expression of ISX (as pointed by arrows) in pancreatic tumor specimens of PDAC patients as determined by immunohistochemical (IHC) analysis. (C) Association of *ISX* to PDAC disease phenotype and survival analysis in patients. (Ci) Box-plots show the copy number of *ISX* gene in PDAC patient speciemns from the analysis of oncomine database. (Cii) The line graph shows the Kaplan-Meier analysis for the survival probability of PDAC male and female patients exhibiting varied *ISX* expression. (Di) Histogram showing the effect of *ISX* suppression on (Bi) cell migration (scratch wound assay) and (Dii) invasiveness potential (chemoinvasion assay) of metastatic cell models (HI-PancM and AsPC1) grown under either hypoxia or normoxia. Control cells were transfected with scrambled siRNA. Test group of cells were transfected with *ISX*-specific siRNA (150 nM). (E) The regulation of *MMP2, VEGF*, and NFκB by ISX in PDAC models as determined by luciferase-based reporter assays. (Ei-ii) Histograms showing the *MMP2* promoter activity, (Ei-ii) histograms showing the *VEGF* promoter activity, and (Ev-vi) histograms showing the transcriptional activity of NFκB (*NFκB-responsive element*) activity in metastatic cells grown under either hypoxia or normoxia conditions (HI-PancM and UMPDC2). (F) Histograms showing the effect of ISX-suppression on the cell cycle (at Sub-G0/G1, G1 and G2/M stages) distribution of metastatic ASPC1 growing under either (Fi) hypoxia or (Fii) normoxia conditions.

stages of PDAC progression. Importantly, each comes from mice with an identical genetic background; therefore, the differences in molecular/cellular landscape are due to PDAC progression, not differences in driver mutations.

The activating K-ras mutation promotes persistent signaling to downstream effectors molecules which in turn results in enhanced stimulation of proliferative pathways such as PI3K/AKT, the mitogen-activated protein kinase (MAPK), and NFκB, thus conferring a growth advantage to the cancer cells [19]. Akt activation has been reported to correlate with worse prognosis in PDAC patients [49]. NFκB is reported to be constitutively activated in 70% of PDAC cases [49]. Our models rightly capture these two important molecular events (of NFκB and Akt activation) during the PDAC disease progression. However, the noticeable observation in our study is that no activation of either Akt or NFκB was found in model representing localized PDAC, whereas it was remarkable in models representing invasive and metastatic stages of disease. This observation is clinically significant because it identifies an accurate stage of disease suitable for therapies targeting NFκB or Akt pathways to treat PDAC. This observation also could be an explanation for the failure of AKT or NFκB-targeting therapies in patients receiving the therapies irrespective of disease stage. However, it is to be noted that these observations are relevant to the patients exhibiting *K-ras* and as INK4A/p16 aberrations. Genomic instability is an important molecular event for acquiring of a particular phenotypes by neoplastic cells during the progression of disease [50]. Campbell et al. reported that genomic instability that frequently persists after cancer dissemination is required for pancreatic primary tumor cells to acquire divergent phenotypes during progression of disease [51]. One of the major cell organelles that is reported to contribute to the genomic stability (by forming bipolar spindles and segregating chromosomes) in neoplastic cells is the centrosome [22,23]. It was Theodor Boveri almost 100 years ago who suggested that extra centrosomes would lead to multipolar cell divisions, resulting in genetic instability and malignant transformation [52]. Numerous studies show that the centrosome amplification correlates with high-grade tumors and poor prognosis [49]. Notably, some reports have shown that centrosome amplification was detectable in some early low-grade lesions, giving weight to the argument that centrosome amplification could drive tumorigenesis [51–53]. We observed a remarkable change in the centrosome numbers in PDAC cell models representing different stages of PDAC. Our study supports the notion that occurrence of a change in centrosome number during progressive stages of PDAC could be a driver for the development of aggressive PDAC phenotype via the formation of transient multipolar mitotic spindles. Another factor that has emerged as an important contributor to the genomic instability is the cilia [31]. Cilia serve as a cellular "antenna" that transmits an indispensable signaling pathways in the cell. Loss of cilia is commonly observed during the progression of large number of cancers. As is the case with many cancers, primary cilia are absent from the majority of human PanIN and PDAC lesions. Our murine and human PDAC model faithfully recapitulates the reported clinical condition showing the gradual loss of primary cilia with the progression of disease from localized to metastatic phenotype.

One of the key factors that correlates with poor survival of patients with PDAC is the extent of hypoxic areas within the tumor tissue [54]. The adaptation of pancreatic tumor cells to deficient oxygen to tumor tissues is reported to promote the induction of an invasive and treatment-resistant phenotype, thus triggering metastases at an early stage of tumor development [54]. Notably, the growth pattern and aggressive behavior of HI-Panc-L, HI-Panc-I, HI-Panc-M, and UM-PDC models under hypoxia conditions match the clinical condition in PDAC patients who exhibit a quick progression of disease after diagnosis. Therefore, it is desirable that therapies be identified which perform better under hypoxic conditions and that biomarker signatures be identified which are detectable under hypoxic conditions. This would require progression models which are of same genetic background and grow under similar hypoxic conditions.

We performed RNA sequencing of progression models grown under hypoxic conditions and identified important genetic changes occurring within hypoxia tumor cells at different stages of PDAC disease. We identified several genes which either showed i) a consistent change in expression during the progressive stages of PDAC from localized to metastatic or ii) a significant change only at one certain stage of disease. The significance of this study is that using RNA sequencing information, we identified *ISX* as a hypoxia-responsive gene that plays an important role in the invasiveness of metastatic PDAC cells [8]. *ISX* (aliases Pix1, RAXLX, intestine specific homeobox) belongs to homeobox family and is a transcription factor involved in early embryonic development. The string analysis (10.5.string version) shows that ISX transcriptional factor forms a close network with homeobox proteins (LDB1, LDB2, LEUTX, LHX3, LHX4). ISX is reported to regulate high-density lipoprotein receptor and cholesterol transporter scavenger receptor in the intestines of mice [37,55,56]. Hsu et al. and Wang et al. reported that ISX factor induces the inflammation, binds to the promoter region of cyclin D1, and induces the expression of E2F1 in liver cells [56].

An important observation of this study is that *ISX*-positive hypoxic PDAC tumor cells harbor enriched M2 macrophages related gene set. It is to be noted that M2-polarized macrophages are known i) to promote cancer progression and ii) be responsive to IL-6 cytokine. Based on the integrated genomic data and GSEA of hypoxic models, it is speculated that enrichment of *ISX* (resulting in modulation of tumor suppressors and M2-macrophage pathway) under hypoxic conditions could be an underlying mechanism for metastatic progression of PDAC in patients. Therefore, we suggest that *ISX*-GSEA molecular signature has a potential to be developed as a PDAC progression biomarker. However, this warrants further investigation in clinical settings. The significance of *ISX* contributing to metastasis progression in PDAC could be ascertained from our data showing i) the dependence of metastatic genes *VEGF, MMP2,* and *NFκB* on the expression of *ISX* in tumor cells and ii) *TCGA* clinical data showing a positive correlation of *ISX* copy number to the high-grade metastatic PDAC.

Because targeting of ISX caused an inhibition in the transcription of metastatic genes, we suggest that ISX could be exploited as a therapeutic target for treating metastatic PDAC. Our data open an opportunity to target ISX by potential therapies such as small molecule inhibitors, peptides, and chimeric RNA. Efforts are under way (in our laboratory) to identify the small molecule inhibitors of ISX. To summarize, this study i) provides a novel tool to study the PDAC disease and test future therapies and ii) identifies *ISX* as a progression biomarker as well as therapeutic target for PDAC in humans.

Supplementary data to this article can be found online at https://doi.org/10.1016/j.tranon.2019.05.002.

Acknowledgement

This study was supported by an investigator award from American Institute of Cancer Research (AICR application #09A074) to author (M. S.). The author (M.S.) is supported by US PHS grants (CA193739,

CA184685, and CA184685-02S1). We thank Dr. Anindya Bagchi and the genomic center of UoM for helping in RNA sequencing of models. We thank Lyn Oseath (Shared Resources, Masonic Cancer Center) for helping in karyotyping of cells models. We thank Neelofar Jan and Mudassir M. Banday for providing help in animal and qPCR validation studies, respectively.

References

[1] Vaccaro V, Sperduti I, Vari S, Bria E, Melisi D, Garufi C, Nuzzo C, Scarpa A, Tortora G, and Cognetti F, et al (2015). Metastatic pancreatic cancer: is there a light at the end of the tunnel? *World J Gastroenterol* **21**, 4788–4801.

[2] Baschnagel A, Shah C, Margolis J, Nadeau L, Stein J, Jury R, and Robertson JM (2012). Survival after chemoradiation in resected pancreatic cancer: the impact of adjuvant gemcitabine. *Int J Radiat Oncol Biol Phys* **83**, e331–e335.

[3] Crane CH, Abbruzzese JL, Evans DB, Wolff RA, Ballo MT, Delclos M, Milas L, Mason K, Charnsangavej C, and Pisters PW, et al (2002). Is the therapeutic index better with gemcitabine-based chemoradiation than with 5-fluorouracil-based chemoradiation in locally advanced pancreatic cancer? *Int J Radiat Oncol Biol Phys* **52**, 1293–1302.

[4] Makohon-Moore A and Iacobuzio-Donahue CA (2016). Pancreatic cancer biology and genetics from an evolutionary perspective. *Nat Rev Cancer* **16**, 553–565.

[5] Koliopanos A, Avgerinos C, Paraskeva C, Touloumis Z, Kelgiorgi D, and Dervenis C (2008). Molecular aspects of carcinogenesis in pancreatic cancer. *Hepatobiliary Pancreat Dis Int* **7**, 345–356.

[6] Hwang CI, Boj SF, Clevers H, and Tuveson DA (2016). Preclinical models of pancreatic ductal adenocarcinoma. *J Pathol* **238**, 197–204.

[7] Oldfield LE, Connor AA, and Gallinger S (2017). Molecular events in the natural history of pancreatic cancer. *Trends Cancer* **3**, 336–346.

[8] Christensen KL, Patrick AN, McCoy EL, and Ford HL (2008). The six family of homeobox genes in development and cancer. *Adv Cancer Res* **101**, 93–126.

[9] Hingorani SR, Petricoin EF, Maitra A, Rajapakse V, King C, Jacobetz MA, Ross S, Conrads TP, Veenstra TD, and Hitt BA, et al (2003). Preinvasive and invasive ductal pancreatic cancer and its early detection in the mouse. *Cancer Cell* **4**, 437–450.

[10] Aguirre AJ, Bardeesy N, Sinha M, Lopez L, Tuveson DA, Horner J, Redston MS, and DePinho RA (2003). Activated Kras and Ink4a/Arf deficiency cooperate to produce metastatic pancreatic ductal adenocarcinoma. *Genes Dev* **17**, 3112–3126.

[11] Siddique HR, Adhami VM, Parray A, Johnson JJ, Siddiqui IA, Shekhani MT, Murtaza I, Ambartsumian N, Konety BR, and Mukhtar H, et al (2013). The S100A4 oncoprotein promotes prostate tumorigenesis in a transgenic mouse model: regulating NFkappaB through the RAGE receptor. *Genes Cancer* **4**, 224–234.

[12] Griffin CA, Morsberger L, Hawkins AL, Haddadin M, Patel A, Ried T, Schrock E, Perlman EJ, and Jaffee E (2007). Molecular cytogenetic characterization of pancreas cancer cell lines reveals high complexity chromosomal alterations. *Cytogenet Genome Res* **118**, 148–156.

[13] Saleem M, Murtaza I, Tarapore RS, Suh Y, Adhami VM, Johnson JJ, Siddiqui IA, Khan N, Asim M, and Hafeez BB, et al (2009). Lupeol inhibits proliferation of human prostate cancer cells by targeting beta-catenin signaling. *Carcinogenesis* **30**, 808–817.

[14] Gradilone SA, Radtke BN, Bogert PS, Huang BQ, Gajdos GB, and LaRusso NF (2013). HDAC6 inhibition restores ciliary expression and decreases tumor growth. *Cancer Res* **73**, 2259–2270.

[15] Mansini AP, Lorenzo Pisarello MJ, Thelen KM, Cruz-Reyes M, Peixoto E, Jin S, Howard BN, Trussoni CE, Gajdos GB, and LaRusso NF, et al (2018). MicroRNA (miR)-433 and miR-22 dysregulations induce histone-deacetylase-6 overexpression and ciliary loss in cholangiocarcinoma. *Hepatology* **68**, 561–573.

[16] Subramanian A, Tamayo P, Mootha VK, Mukherjee S, Ebert BL, Gillette MA, Paulovich A, Pomeroy SL, Golub TR, and Lander ES, et al (2005). Gene set enrichment analysis: a knowledge-based approach for interpreting genome-wide expression profiles. *Proc Natl Acad Sci U S A* **102**, 15545–15550.

[17] Chandrashekar DS, Bashel B, Balasubramanya SAH, Creighton CJ, Ponce-Rodriguez I, Chakravarthi B, and Varambally S (2017). UALCAN: a portal for facilitating tumor subgroup gene expression and survival analyses. *Neoplasia* **19**, 649–658.

[18] Bardeesy N, Aguirre AJ, Chu GC, Cheng KH, Lopez LV, Hezel AF, Feng B, Brennan C, Weissleder R, and Mahmood U, et al (2006). Both p16(Ink4a) and the p19(Arf)-p53 pathway constrain progression of pancreatic adenocarcinoma in the mouse. *Proc Natl Acad Sci U S A* **103**, 5947–5952.

[19] Ling J, Kang Y, Zhao R, Xia Q, Lee DF, Chang Z, Li J, Peng B, Fleming JB, and Wang H, et al (2012). KrasG12D-induced IKK2/beta/NF-kappaB activation by IL-1alpha and p62 feedforward loops is required for development of pancreatic ductal adenocarcinoma. *Cancer Cell* **21**, 105–120.

[20] Stanger BZ, Stiles B, Lauwers GY, Bardeesy N, Mendoza M, Wang Y, Greenwood A, Cheng KH, McLaughlin M, and Brown D, et al (2005). Pten constrains centroacinar cell expansion and malignant transformation in the pancreas. *Cancer Cell* **8**, 185–195.

[21] Itakura J, Ishiwata T, Friess H, Fujii H, Matsumoto Y, Buchler MW, and Korc M (1997). Enhanced expression of vascular endothelial growth factor in human pancreatic cancer correlates with local disease progression. *Clin Cancer Res* **3**, 1309–1316.

[22] Andor N, Maley CC, and Ji HP (2017). Genomic instability in cancer: teetering on the limit of tolerance. *Cancer Res* **77**, 2179–2185.

[23] Thompson SL and Compton DA (2008). Examining the link between chromosomal instability and aneuploidy in human cells. *J Cell Biol* **180**, 665–672.

[24] Ganem NJ, Godinho SA, and Pellman D (2009). A mechanism linking extra centrosomes to chromosomal instability. *Nature* **460**, 278–282.

[25] Hinchcliffe EH (2014). Centrosomes and the art of mitotic spindle maintenance. *Int Rev Cell Mol Biol* **313**, 179–217.

[26] Hornick JE, Mader CC, Tribble EK, Bagne CC, Vaughan KT, Shaw SL, and Hinchcliffe EH (2011). Amphiastral mitotic spindle assembly in vertebrate cells lacking centrosomes. *Curr Biol* **21**, 598–605.

[27] Silkworth WT, Nardi IK, Scholl LM, and Cimini D (2009). Multipolar spindle pole coalescence is a major source of kinetochore mis-attachment and chromosome mis-segregation in cancer cells. *PLoS One* **4**e6564.

[28] Silio V, Redondo-Munoz J, and Carrera AC (2012). Phosphoinositide 3-kinase beta regulates chromosome segregation in mitosis. *Mol Biol Cell* **23**, 4526–4542.

[29] Liu D, Vader G, Vromans MJ, Lampson MA, and Lens SM (2009). Sensing chromosome bi-orientation by spatial separation of aurora B kinase from kinetochore substrates. *Science* **323**, 1350–1353.

[30] Turinetto V and Giachino C (2015). Multiple facets of histone variant H2AX: a DNA double-strand-break marker with several biological functions. *Nucleic Acids Res* **43**, 2489–2498.

[31] Izawa I, Goto H, Kasahara K, and Inagaki M (2015). Current topics of functional links between primary cilia and cell cycle. *Cilia* **4**, 12.

[32] Gradilone SA, Pisarello MJL, and LaRusso NF (2017). Primary cilia in tumor biology: the primary cilium as a therapeutic target in cholangiocarcinoma. *Curr Drug Targets* **18**, 958–963.

[33] Kobayashi T and Itoh H (2017). Loss of a primary cilium in PDAC. *Cell Cycle* **16**, 817–818.

[34] Caspary T, Marazziti D, and Berbari NF (2016). Methods for visualization of neuronal cilia. *Methods Mol Biol* **1454**, 203–214.

[35] Perdiz D, Mackeh R, Pous C, and Baillet A (2011). The ins and outs of tubulin acetylation: more than just a post-translational modification? *Cell Signal* **23**, 763–771.

[36] Vasseur S, Tomasini R, Tournaire R, and Iovanna JL (2010). Hypoxia induced tumor metabolic switch contributes to pancreatic cancer aggressiveness. *Cancers (Basel)* **2**, 2138–2152.

[37] Lobo GP, Hessel S, Eichinger A, Noy N, Moise AR, Wyss A, Palczewski K, and von Lintig J (2010). ISX is a retinoic acid-sensitive gatekeeper that controls intestinal beta,beta-carotene absorption and vitamin A production. *FASEB J* **24**, 1656–1666.

[38] Widjaja-Adhi MAK, Palczewski G, Dale K, Knauss EA, Kelly ME, Golczak M, Levine AD, and von Lintig J (2017). Transcription factor ISX mediates the cross talk between diet and immunity. *Proc Natl Acad Sci U S A* **114**, 11530–11535.

[39] Mootha VK, Lindgren CM, Eriksson KF, Subramanian A, Sihag S, Lehar J, Puigserver P, Carlsson E, Ridderstrale M, and Laurila E, et al (2003). PGC-1alpha-responsive genes involved in oxidative phosphorylation are coordinately downregulated in human diabetes. *Nat Genet* **34**, 267–273.

[40] Banerjee-Basu S and Baxevanis AD (2001). Molecular evolution of the homeodomain family of transcription factors. *Nucleic Acids Res* **29**, 3258–3269.

[41] Choi MY, Romer AI, Hu M, Lepourcelet M, Mechoor A, Yesilaltay A, Krieger M, Gray PA, and Shivdasani RA (2006). A dynamic expression survey identifies transcription factors relevant in mouse digestive tract development. *Development* **133**, 4119–4129.

[42] Rhodes DR, Yu J, Shanker K, Deshpande N, Varambally R, Ghosh D, Barrette T, Pandey A, and Chinnaiyan AM (2004). ONCOMINE: a cancer microarray database and integrated data-mining platform. *Neoplasia* **6**, 1–6.

[43] Parray A, Siddique HR, Kuriger JK, Mishra SK, Rhim JS, Nelson HH, Aburatani H, Konety BR, Koochekpour S, and Saleem M (2014). ROBO1, a tumor suppressor and critical molecular barrier for localized tumor cells to acquire invasive phenotype: study in African-American and Caucasian prostate cancer models. *Int J Cancer* **135**, 2493–2506.

[44] Lekstan A, Lampe P, Lewin-Kowalik J, Olakowski M, Jablonska B, Labuzek K, Jedrzejowska-Szypulka H, Olakowska E, Gorka D, and Filip I, et al (2012). Concentrations and activities of metalloproteinases 2 and 9 and their inhibitors (TIMPS) in chronic pancreatitis and pancreatic adenocarcinoma. *J Physiol Pharmacol* **63**, 589–599.

[45] Roy R, Zurakowski D, Wischhusen J, Frauenhoffer C, Hooshmand S, Kulke M, and Moses MA (2014). Urinary TIMP-1 and MMP-2 levels detect the presence of pancreatic malignancies. *Br J Cancer* **111**, 1772–1779.

[46] Hogendorf P, Durczynski A, Kumor A, and Strzelczyk J (2014). Pancreatic head carcinoma and vascular endothelial growth factor (VEGF-A) concentration in portal blood: its association with cancer grade, tumor size and probably poor prognosis. *Arch Med Sci* **10**, 288–293.

[47] Tabruyn SP, Griffioen AW, and NF-kappa B (2008). a new player in angiostatic therapy. *Angiogenesis* **11**, 101–106.

[48] Habbe N, Shi G, Meguid RA, Fendrich V, Esni F, Chen H, Feldmann G, Stoffers DA, Konieczny SF, and Leach SD, et al (2008). Spontaneous induction of murine pancreatic intraepithelial neoplasia (mPanIN) by acinar cell targeting of oncogenic Kras in adult mice. *Proc Natl Acad Sci U S A* **105**, 18913–18918.

[49] Weichert W, Boehm M, Gekeler V, Bahra M, Langrehr J, Neuhaus P, Denkert C, Imre G, Weller C, and Hofmann HP, et al (2007). High expression of RelA/p65 is associated with activation of nuclear factor-kappaB-dependent signaling in pancreatic cancer and marks a patient population with poor prognosis. *Br J Cancer* **97**, 523–530.

[50] Campbell PJ, Yachida S, Mudie LJ, Stephens PJ, Pleasance ED, Stebbings LA, Morsberger LA, Latimer C, McLaren S, and Lin ML, et al (2010). The patterns and dynamics of genomic instability in metastatic pancreatic cancer. *Nature* **467**, 1109–1113.

[51] Hinchcliffe EH and Sluder G (2001). "It takes two to tango": understanding how centrosome duplication is regulated throughout the cell cycle. *Genes Dev* **15**, 1167–1181.

[52] Holland AJ and Cleveland DW (2009). Boveri revisited: chromosomal instability, aneuploidy and tumorigenesis. *Nat Rev Mol Cell Biol* **10**, 478–487.

[53] Brinkley BR (2001). Managing the centrosome numbers game: from chaos to stability in cancer cell division. *Trends Cell Biol* **11**, 18–21.

[54] Erkan M, Kurtoglu M, and Kleeff J (2016). The role of hypoxia in pancreatic cancer: a potential therapeutic target? *Expert Rev Gastroenterol Hepatol* **10**, 301–316.

[55] Hsu SH, Wang LT, Lee KT, Chen YL, Liu KY, Suen JL, Chai CY, and Wang SN (2013). Proinflammatory homeobox gene, ISX, regulates tumor growth and survival in hepatocellular carcinoma. *Cancer Res* **73**, 508–518.

[56] Wang SN, Wang LT, Sun DP, Chai CY, Hsi E, Kuo HT, Yokoyama KK, and Hsu SH (2016). Intestine-specific homeobox (ISX) upregulates E2F1 expression and related oncogenic activities in HCC. *Oncotarget* **7**, 36924–36939.